PdAuAg alloy nanoparticles on nickel foam as anode for passive air-breathing formate fuel cell

Bowei Pan, [1,2] Fuyi Chen, [1,2,z] Junpeng Wang, [1,2] Quan Tang, [1,2] Longfei Guo, [1,2] Tao Jin, [1,2] Chenxi Peng, [1,2] Liang An[3] and Yu Chen [4]

[1] State Key Laboratory of Solidification Processing, Northwestern Polytechnical University, Xi'an 710072, China
[2]School of Materials Science and Engineering, Northwestern Polytechnical University, Xi'an, 710072, China
[3]Department of Mechanical Engineering, The Hong Kong Polytechnic University, Hung Hom, Kowloon, Hong Kong SAR, China
[4]Department of Physics, University of Strathclyde, John Anderson Building, 107 Rottenrow, Glasgow G4 0NG. UK
[z] E-mail: fuyichen@nwpu.edu.cn

Abstract: A passive air-breathing formate fuel cell with PdAuAg alloy nanoparticles supported on the carbon nanotube (CNT) pasted on nickel foam (NF) as anode is reported in this work. With optimization, a maximum power density of 16 mW cm^{-2} with PdAuAg/CNT on NF as anode is achieved, which is 2.2 time of that achieved by using commercial Pd/C on NF (7.3 mW cm^{-2}). Furthermore, the cell with PdAuAg/CNT on NF as anode can steadily discharge at 5 mA cm^{-2} for more than 28 hours continuously. This is, to our knowledge, the best performance of passive air-breathing formate fuel cells reported so far and PdAuAg/CNT on NF as anode can be considered as the state-of-the-art for the passive air-breathing formate fuel cell. These results suggested that the PdAuAg/CNT catalyst probably provides an alternative avenue for developing the anode electrocatalysts for passive air-breathing formate fuel cell applications.

Introduction

Direct liquid fuel cells (DLFCs) have received great attention[1-4] in the last decade because of the increased demand for portable electronic devices. Especially formate liquid fuels without formation of catalyst poison in an alkaline environment[5-7] are highly desirable. Among all kinds of liquid fuels, formate fuel has attracted increasing attention[8-10] due to its advantages superior to other fuels. Firstly, formate oxidation is extremely easy under alkaline conditions, especially on Pd[11, 12]. Secondly, the theoretical potential of formate is 1.45V (vs. $E_{methanol}$=1.21V)[13, 14]. Thirdly, the oxidation of formate in an alkaline media doesn't cause CO poisoning[15]. Finally, formate can be stored and transported in a solid state[16]. However, formate oxidation reaction (FOR) plays a dominant role in the performance of formate fuel cells, and the slow kinetics of the FOR on the anode limits the further development and commercial exploitation[17]. For formate oxidation reaction, Pd is considered to be a catalyst with high activity, stability and resistance to CO poisoning and exceeds Pt[18, 19]. We have previously studied[20] the ternary PdAuAg alloy nanoparticles supported on the carbon nanotube (CNT) as a catalyst for formate oxidation reaction and demonstrated its outstanding electrocatalytic performance.

Until now, the external pumps are generally required to drive the fuel and oxidant flow in most formate fuel cells[21]. However, the use of the pump not only reduces the specific energy output but also prevents further miniaturization and portability of the formate fuel cells[22-24]. The passive fuel cells play an important role in the fuel cell community because it is unlikely that pumps can be employed in portable devices, so the performance of passive fuel cells brings the community's research an important step closer to implementation. Hence, passive air-breathing formate fuel cells were considered as promising formate fuel cells in flexible electronic[25], including portable energy conversion devices, wearable and disposable devices[26]. However, several challenges retard the commercialization of passive air-breathing formate fuel cells technology, including the mass/ion transport in the catalyst layer and poor fuel cell performance[27-29].

To improve the mass/ion transport in the catalyst layer and fuel cell performance, nickel foam structures have been extensively studied to promote the species transport in other liquid fuel cells[30]. Conventional dual-layer electrode is widely used in liquid fuel cells, consisting of a diffusion layer and a catalyst layer[31]. This dual-layer structure has a very dense catalyst layer that creates a barrier for mass/ion transport[32]. Therefore, nickel foam with three-dimensional nano-porous structure has attracted the attention of researchers to improve the fuel cell performance. Li et al.[33] studied the conventional dual-layer anode and nickel foam anode in direct ethanol fuel cells. The results showed that a nickel foam anode has a peak power density 1.5 time of that from a dual-layer anode. Liu et al.[23] demonstrated a direct methanol fuel cell with a peak power density up to 73.5 mW cm^{2-} by using nickel foam as anode and cathode. Li et al[7] prepared a 3D porous electrodes with Pd-Au alloy coated nickel foam, the direct formate fuel cell can yield an open-circuit voltage of 1.51 V and a peak power density of 331 mW cm^{2-}, which are higher than the state-of-the-art anion-exchange membrane direct formate fuel cell.

In light of that, a passive air-breathing formate fuel cell with nickel foam electrode was proposed, where PdAuAg alloy nanoparticles supported on carbon nanotube were pasted on the nickel foam matrix surface. The nickel foam was employed as both the gases and liquids channel to achieve the higher mass/ion transport[34]. The pump and flow control systems can be eliminated, which will significantly reduce fuel cell complexity[35]. In this work, three types of nickel foam electrodes were fabricated using different preparation methods for passive air-breathing formate fuel cell; namely, (1) the commercial Pd/C nanoparticles pasted on nickel foam (Pd/C on NF) as anode; (2) the PdAuAg alloy nanoparticles supported on the carbon nanotube pasted on nickel foam (PdAuAg/CNT on NF) via a dip-coating method as anode and (3) PdAuAg nanoparticles deposited on nickel foam (PdAuAg on NF) via reduction reaction deposition as anode for passive air-breathing formate fuel cells. The results demonstrated that the PdAuAg/CNT on NF as anode possesses the highest peak power density, higher than those achieved by using commercial Pd/C on NF and PdAuAg on NF. In this study, for the first time, we propose a passive air-breathing formate fuel cell with home-made PdAuAg/CNT nanoparticles pasted on nickel foam as anode. To the best of our knowledge, this PdAuAg/CNT on nickel foam produces the highest peak power density among all reported passive air-breathing formate fuel cell as summarized in Table 1. The results elucidated that the proposed fuel cell might be a good alternative to the battery for powering portable electronics.

Experimental

Materials

Pd/C (30 wt.%) was purchased from Aladdin Industrial Corporation. Pt/C (20 wt.%) was purchased from Shanghai Hesen Electric limited company. The anion-exchange membrane was Fumapem AM-40. Ni foams with a purity of 99.8% (pore per inch: 120, density: 370 g m^{-2}, average pore size: 500 um, thickness: 1 mm), were purchased from Taiyuan Lizhiyuan Battery Material limited company. The PdAuAg alloy nanoparticles supported on the carbon nanotube was prepared using a method described in our previous work[20].

Electrode preparation

To prepare the cathode electrodes with commercial Pt/C pasted on nickel foam, an emulsion of 10 mg Pt/C and 10 mg Nafion solution (Nafion, 5 wt.%) in ethanol was first obtained by ultrasonic dispersion. The as-prepared slurry was then coated on nickel foam and dried for 3 h. The cathode electrode was composed of a gas diffusion layer (preparation method described in our previous work) and the catalyst on NF layer. The cathode electrode was achieved by pressing gas diffusion layer and the coated nickel foam together at a pressure of 10 MPa for 30 seconds.

Four types anode electrodes were prepared in this study, namely the commercial Pd/C nanoparticles pasted on nickel foam (Pd/C on NF), PdAuAg/CNT nanoparticles pasted on nickel foam (PdAuAg/CNT on NF), PdAuAg/CNT nanoparticles pasted on carbon paper (PdAuAg/CNT on CP) and PdAuAg nanoparticles depositing on nickel foam (PdAuAg on NF). The nickel foams were firstly cleaned using acetone and dilute sulphuric acid (5%) to remove the oils and oxides. The nickel foam was immersed in 3 mM $Pd(NO_3)_2$, 3 mM $HAuCl_4$ and 1 mM $AgNO_3$ mixed solution for 30 minutes, the as-prepared PdAuAg on NF was washed in the double distilled water and dried with N_2. The Pd/C on NF, PdAuAg/CNT on NF and PdAuAg/CNT on CP were prepared as follows: an emulsion of 10 mg Pd/C or PdAuAg/CNT and 10 mg Nafion solution (Nafion, 5 wt.%) in ethanol was obtained by ultrasonic dispersion. The as-prepared slurry was then pasted on nickel foam or carbon paper and dried for 3 h. The anode electrode was achieved by pressing coated nickel foam at a pressure of 10 MPa for 30 seconds.

Fuel cell test

The anode electrode, anion-exchange membrane and cathode electrode were assembled into a fuel cell, and its performance was measured by discharging tests and stability tests using a battery testing system (Neware Technology Limited Company, Shenzhen, China). The cathode side was air, and the anode side was 4 M KOH + 5 M HCOOK aqueous solution. In addition, CHI 660C electrochemical workstation (Chenhua, China) was used for the electrochemical impendence spectra (EIS) test.

Results and Discussion

Fuel cell setup and working principle

Fig. 1 and Fig.2 show the schematic diagram and the photograph of a passive air-breathing formate fuel cell that consists of a membrane electrode assembly (MEA) sandwiched between two anode fuel and cathode air fields. The MEA is composed of an

anode electrode, an anion-exchange membrane and a cathode electrode. On the anode side, the formate in the potassium hydroxide solution flows from the tank through coated nickel foam is oxidized to produce electrons, water, and carbonate ions[36].

$$\text{Anode: } HCOO^- + 3OH^- \rightarrow CO_3^{2-} + 2H_2O + 2e^- \quad (E_a = -1.05\ V) \tag{1}$$

On the cathode side, the oxygen passes through the cathode diffusion layer to the cathode catalyst layer, where oxygen with the electrons generated by formate oxidation through the external circuit to the cathode side takes place an oxygen reduction reaction (ORR) to produce hydroxide ions[37].

$$\text{Cathode: } \frac{1}{2}O_2 + H_2O + 2e^- \rightarrow 2OH^- \quad (E_c = 0.40\ V) \tag{2}$$

And then, hydroxide ions generated by the cathode reaction are transported through the anion exchange membrane to the anode catalyst layer for continuous formate oxidation process[38]. Thereby, the overall reaction in the formate fuel cell is:

$$\text{Overall: } HCOO^- + \frac{1}{2}O_2 + OH^- \rightarrow CO_3^{2-} + H_2O \quad (E_{cell} = 1.45\ V) \tag{3}$$

Effect of the hydroxide-ion concentration

Hydroxide-ion has to be added into the formate solution not only because the ionic conductivity of the anion-exchange membrane is low[39], but also because the addition of hydroxide-ion is found to further enhance the electrochemical kinetics of the FOR[40, 41]. Hence, the effect of the hydroxide-ion concentration is studied and presented in Fig. 3. Fig. 3 shows the effect of 0, 2, 4 and 6 M KOH with 5 M HCOOK as the anode fuel operates at 25 ℃ with air at the cathode, increasing the hydroxide-ion concentration can improve the cell performance. For example, the cell voltage increases from 0.79 V to 0.98 V and the peak power density increases from 9.8 mW cm^{-2} to 16 mW cm^{-2} when the hydroxide-ion concentration added from 2 M to 4 M. This is because the enhancement of hydroxide-ion concentration not only improves the electrochemical kinetics of FOR, but also increases the transfer rate of hydroxide ions[42]. The cell performance is rather low when the HCOOK without any addition of KOH, it means that the fuel cell requires some hydroxide-ion to be mixed with the HCOOK because they are a reactant in the oxidation of the fuel, so hydroxide-ion mixed with the HCOOK will increase the cell efficiency[43]. It is important to note in Fig. 3 that, although the KOH increases from 4 M to 6 M, the cell performance is not changed much which is caused by the mass-transport limitation of hydroxide-ion and anion competitive adsorption effect. The behavior of the polarization curves with the change of KOH concentration is further examined by the EIS test. Figure 4 shows the different curve types of Nyquist plots at low frequency, the yellow, blue and red lines represent Warburg-type, T-type and O-type. The curve of Warburg-type at low frequency is a straight line at an Angle of 45 degrees from the abscissa, which is commonly used in the analysis of electrode process dynamics, double layers, and diffusion. The T-type curve at low frequency shows an Angle greater than 45 degrees with the abscissa, and then upward warping, which is commonly used in the analysis of conductive polymers, metal corrosion and protection and fuel cells. The O-type curve appears like a semicircle at low frequency, which is commonly used in the analysis of Li-ion batteries, fuel cells and catalysis. Comparing Figures 5 and 7 with Figure 4,

the Nyquist plots of this work are consistent with T-type, indicating that the transfer rate is controlled by the fuel concentration in the fuel cell. An equivalent electric circuit (Fig. 5(a), inset) is utilized to fit the Nyquist plot. Fig. 5(a) depicts the Nyquist plots of the passive air-breathing formate fuel cell at various KOH concentrations with 5 M HCOOK as the anode fuel operates at 25 ℃ with air at the cathode. When the KOH increased from 0 M to 2 and 4 M, the arc of the impedance spectra decreased in high-frequency region, it confirms that the charge transfer of the electrochemical reaction was enhanced with an added KOH, but when the KOH concentration was further increased to 6 M, the diameter was increased due to the competitive adsorption, this corresponds to the variations in the Bode plot (Fig. 5(b)). So a concentration of 4 M KOH is optimal, which will be used in rest of the experiments.

Effect of the formate concentration

For a passive air-breathing formate fuel cell, the formate concentration in the fuel solution becomes important parameter to achieve high cell performance. So the effect of the formate concentration on the cell performance is investigated and presented in Fig. 6 with the fuel cell operated at 25 ℃ using air at the cathode and 4 M KOH with varied concentrations of formate fuel at the anode. It shows that an enhancement in the formate concentration from 1 M to 5 M increases the cell voltage and the peak power density, such as the cell voltage increase from 0.75 V to 0.98 V and the peak power density increase from 6 mW cm^{-2} to 16 mW cm^{-2}. It is clear that the improvement in cell performance is attributed to two aspects, the electrochemical kinetics of FOR is improved with the increase of formate concentration[44]; the formate transfer rate to the anode catalyst layer is accelerated with the increase of formate concentration. When the formate concentration was increased to 7 M HCOOK, the cell performance remained stable comparing with the formate concentration of 5 M HCOOK, which is probably because redundant formate adsorbed on the catalyst surface blocks the formate oxidation reaction further. Fig. 7 shows the Nyquist and Bode plots of the passive air-breathing formate fuel cell at different formate concentration with 4 M KOH operates at 25 ℃ with air at the cathode. It is indicates that the impedance is declined first and then increased with the formate concentration is from 1 M, 3 M, 5 M to 7M. The results confirm that the FOR is accelerated by increase the formate concentration, but too high formate concentration will increase the mass transport resistance of formate. So a concentration of 5 M HCOOK is determined to be optimal in rest of the experiments.

Effect of the operation temperature

Formate fuel cells utilizing an anion exchange membrane is usually operated at a temperature above ambient temperature in order to achieve better cell performance[45]. For a passive air-breathing formate fuel cell, it would be better to run at or near ambient temperature[46]. Fig. 8 shows the results of cell performance at various temperatures with air at the cathode and 4 M KOH + 5 M HCOOK at the anode. It found that the peak power density increased from 16 mW cm^{-2} at 25 ℃ to 19.5 mW cm^{-2} at 50 ℃ and 20.8 mW cm^{-2} at 75 ℃. The improved performance is expected as both the conductivity of the membrane and reaction kinetics are all temperature-dependent[47]. However, the application of passive air-breathing formate fuel cells in portable electronic devices would be better off if the fuel cells can be operated at or near ambient temperature, so a temperature of 25 ℃ is determined

to be chosen in rest of the experiments.

Optimization of the passive air-breathing formate fuel cell

In order to optimize the passive air-breathing formate fuel cell, the different types of anode electrodes are used in this formate fuel cell. In our previous work, we used the ternary PdAuAg alloy nanoparticles supported on the carbon nanotube for formate oxidation reaction, which confirmed it is a powerful and stable catalyst. So the different anode electrodes including the PdAuAg alloy nanoparticles supported on the carbon nanotube pasted on nickel foam or carbon paper (PdAuAg/CNT on NF or CP) and the commercial Pd/C nanoparticles pasted on nickel foam (Pd/C on NF) via a dip-coating method, PdAuAg nanoparticles depositing on nickel foam (PdAuAg on NF) via reduction reaction deposition, Pt/C is used at the cathode because it is a very reliable catalyst for the oxygen reduction reaction. Fig. 9 shows the operation of the passive air-breathing formate fuel cell with 4 M KOH + 5 M HCOOK as the anode fuel and electrolyte, air as the cathode oxidant, and the fuel cell operating at 25 ℃. It can be found in Fig. 9 (a) and Table 2 that the fuel cell using PdAuAg/CNT on NF electrode yielded much better performance than other fuel cells. Under these conditions the peak power density is 16 mW cm^{-2} with the maximum current density of 64 mA cm^{-2} and the open-circuit voltage of 0.98 V. The commercial Pd/C has a good catalytic performance for the FOR and formate fuel cell. Here we constructed a formate fuel cell with the commercial Pd/C as anode catalyst and compared its performance with that of the PdAuAg/CNT on NF. As expected, the fuel cell with PdAuAg/CNT on NF electrode exhibits a higher power density and maximum current density than the fuel cell with the commercial Pd/C on NF electrode (Table 2, 7.3 mW cm^{-2} and 30 mA cm^{-2}). This demonstrates that the PdAuAg/CNT on NF electrode is very suitable for the passive air-breathing formate fuel cell.

As shown in Fig. 9 (c) and (d), the power density and maximum current density achieved by using PdAuAg/CNT on CP electrode and PdAuAg on NF electrode are relatively lower than that observed by using PdAuAg/CNT on NF electrode. The reasons for improved performance with the PdAuAg/CNT on NF electrode than with PdAuAg/CNT on CP electrode can be explained as follows, the nickel foam has a special three-dimensional structure, which increases the reactant concentration and mass/ion transport in the catalyst layer during the fuel cell operation, reducing the concentration and activation losses[48]. The better performance of the PdAuAg/CNT on NF than PdAuAg on NF can be attributed to the carbon nanotubes. The carbon nanotures have four roles, firstly, it is conductive and plays an important role in the enrichment and conduction of electrons, secondly, it has many channels leading to its high specific surface area and excellent adsorption properties, thirdly, it keeps the metal particles well dispersed and further modulates the properties of the active site, fourthly, it has good alkali resistance, which is very important for the stability of the catalyst. Hence, these observed results further confirmed the excellent performance of fuel cell with the PdAuAg/CNT on NF electrode.

Stability of cells

Stability is an important factor determining cell performance. The stability is tested by monitoring voltage changes during galvanostatic discharge. The cell voltage is recorded at a constant current of 5 mA cm^{-2}, 10 mA cm^{-2}, 20 mA cm^{-2}, and 30 mA cm^{-2} at 25 ℃ and

ambient atmosphere. Fig. 10 (a) shows the stability test of the cell with the PdAuAg/CNT on NF electrode at the different current densities. The cell with the commercial Pd/C on NF electrode is also tested in the same condition as a reference as shown in Fig. 10 (b). The decline of the voltage is due to the consumption of fuel solution; the fuel solution will be refreshed at this point. As shown in Fig. 10 (a), the voltage of the cell with the PdAuAg/CNT on NF electrode is higher than that with the commercial Pd/C on NF electrode at every current density over the test period. Moreover, the stable time of the cell with the PdAuAg/CNT on NF electrode is also longer than that with the commercial Pd/C on NF electrode at every refresh fuel solution period. The mechanism for the improvement of the stability has four aspects, firstly, a homogeneous distribution of PdAuAg alloy nanoparticles on CNT which resulted in a high active, stable and increased conductivity[49], secondly, PdAuAg alloy nanoparticles are not sintered, oxidized or deformed which are able to supply more accessible active sites and provide higher stability and better resistance to deactivation during formate fuel cell operating conditions[50], thirdly, CNT maintained strong adhesion with PdAuAg alloy nanoparticles and provided strong corrosion resistance, thus it can provide durability[51], fourthly, surface segregation of Pd occurs in formate fuel cell operating environment, which provides more catalytic active sites[20]. The stability tests demonstrate that the cell with the PdAuAg/CNT on NF electrode is highly stable and thus has potential for use in practical passive air-breathing formate fuel cells.

Conclusions

This is the first report of a passive air-breathing formate fuel cell employing the PdAuAg/CNT on NF electrode. When the fuel is operated at 25 ℃ with 4 M KOH and 5 M HCOOK as the anode fuel and air at the cathode, the fuel cell produces 16 mW cm^{-2} of power density, 64 mA cm^{-2} of maximum current density, and the open-circuit voltage of 0.98 V, significantly higher than that found using the cell with the commercial Pd/C on NF electrode. This excellent performance is mainly attributed to the nickel foam of unique three-dimensional structures and the outstanding formate catalyst PdAuAg/CNT nanoalloy. These results indicate that the cell with the PdAuAg/CNT on NF electrode will be a promising candidate for the passive air-breathing formate fuel cell in portable electronics.

Acknowledgments

This work was supported by the National Natural Science Foundation of China (grant no. 51874243, 51271148 and 50971100), the Research Fund of State Key Laboratory of Solidification Processing (NPU), China (Grant no. 2020-TS-02), the Project of Transformation of Scientific and Technological Achievements of NWPU (grant no. 19-2017), and the Open Fund of State Key Laboratory of Advanced Technology for Material Synthesis and Processing (Wuhan University of Technology grant no. 2018-KF-18). We would like to thank the Analytical & Testing Center of Northwestern Polytechnical University for TEM characterizations.

References

1. L. An and R. Chen, *Journal of Power Sources*, **320** 127-139 (2016).
2. F. Abd Lah Halim, T. Tsujiguchi, Y. Osaka, and A. Kodama, *International Journal of Energy Research*, **43** (14), 8070-8084 (2019).

3. M. Ahn and J. Kim, *The Journal of Physical Chemistry C*, **117** (46), 24438-24445 (2013).
4. A. M. Bartrom and J. L. Haan, *Journal of Power Sources*, **214** 68-74 (2012).
5. L. An, T. S. Zhao, Z. H. Chai, P. Tan, and L. Zeng, *International Journal of Hydrogen Energy*, **39** (35), 19869-19876 (2014).
6. L. An, T. S. Zhao, S. Y. Shen, Q. X. Wu, and R. Chen, *International Journal of Hydrogen Energy*, **35** (9), 4329-4335 (2010).
7. Y. Li, Y. He, and W. Yang, *Journal of Power Sources*, **278** 569-573 (2015).
8. E. Antolini and E. R. Gonzalez, *Journal of Power Sources*, **195** (11), 3431-3450 (2010).
9. L. Lan, W. Yang, J. Li, L. Zhang, Q. Fu, and Q. Liao, *ACS Appl Mater Interfaces*, **12** (24), 27095-27103 (2020).
10. Q. Wang, F. Chen, Q. Tang, L. Guo, T. T. Gebremariam, T. Jin, H. Liu, B. Kou, Z. Li, and W. Bian, *Applied Catalysis B: Environmental*, **270** 118861 (2020).
11. J. Bai, Q. Xue, Y. Zhao, J.-X. Jiang, J.-H. Zeng, S.-B. Yin, and Y. Chen, *ACS Sustainable Chemistry & Engineering*, **7** (2), 2830-2836 (2019).
12. A. M. Bartrom, J. Ta, T. Q. Nguyen, J. Her, A. Donovan, and J. L. Haan, *Journal of Power Sources*, **229** 234-238 (2013).
13. Y. Chen, L. Zhuang, and J. Lu, *Chinese Journal of Catalysis*, **28** (10), 870-874 (2007).
14. Y. Jin, F. Chen, T. Jin, L. Guo, and J. Wang, *Journal of Materials Chemistry A*, **8** (48), 25780-25790 (2020).
15. M. Choun, K. Ham, D. Shin, J. K. Lee, and J. Lee, *Catalysis Today*, **295** 26-31 (2017).
16. A. Fazil and R. Chetty, **26** (11), 2380-2387 (2014).
17. P. Forysinski, C. Oloman, S. Kazemi, T. Nickchi, and A. Usgaocar, *Journal of Power Sources*, **414** 366-376 (2019).
18. V. Galvan, D. E. Glass, A. F. Baxter, and G. K. S. Prakash, *ACS Applied Energy Materials*, **2** (10), 7104-7111 (2019).
19. Y. Jin, F. Chen, L. Guo, J. Wang, B. Kou, T. Jin, and H. Liu, *ACS Appl Mater Interfaces*, **12** (23), 26694-26703 (2020).
20. B. Pan, F. Chen, B. Kou, J. Wang, Q. Tang, L. Guo, Q. Wang, Z. Li, W. Bian, and J. Wang, *Nanoscale*, **12** (21), 11659-11671 (2020).
21. X. He, D. Li, Z. Bai, F. Chang, J. Qiao, and L. Yang, *Ionics*, **25** (2019).
22. S. Henning, J. Herranz, and H. A. Gasteiger, *Journal of The Electrochemical Society*, **162** (1), F178-F189 (2015).
23. Y. Liu, C. Shu, Y. Fang, Y. Chen, and Y. Liu, *Journal of Power Sources*, **361** 160-169 (2017).
24. Y. Fang, X. Yang, L. Wang, and Y. Liu, *Electrochimica Acta*, **90** 421-425 (2013).
25. Z. Liu, D. Ye, X. Zhu, S. Wang, R. Chen, Y. Yang, and Q. Liao, *Journal of Power Sources*, **490** 229553 (2021).
26. L. Jin, H. Xu, C. Chen, H. Shang, Y. Wang, C. Wang, and Y. Du, *ACS Appl Mater Interfaces*, **11** (45), 42123-42130 (2019).
27. L. An, L. Zeng, and T. S. Zhao, *International Journal of Hydrogen Energy*, **38** (25), 10602-10606 (2013).
28. L. An, T. S. Zhao, and Y. S. Li, *Renewable and Sustainable Energy Reviews*, **50**

1462-1468 (2015).
29. T. Zhang, X. Zhu, D.-D. Ye, R. Chen, Y. Zhou, and Q. Liao, *Nanoscale,* **12** (39), 20270-20278 (2020).
30. I. Bakos, A. Paszternák, and D. Zitoun, *Electrochimica Acta,* **176** 1074-1082 (2015).
31. L. An, T. S. Zhao, L. Zeng, and X. H. Yan, *International Journal of Hydrogen Energy,* **39** (5), 2320-2324 (2014).
32. J. Jiang and A. Wieckowski, *Electrochemistry Communications,* **18** 41-43 (2012).
33. Y. S. Li and T. S. Zhao, *International Journal of Hydrogen Energy,* **36** (13), 7707-7713 (2011).
34. Q. Qin, J. Xie, Q. Dong, G. Yu, and H. Chen, *New Journal of Chemistry,* **43** (48), 19242-19252 (2019).
35. S. Sasidharan, G. Anilkumar, T. Tamaki, and T. Yamaguchi, *ChemCatChem,* (2019).
36. K. Tran, T. Q. Nguyen, A. M. Bartrom, A. Sadiki, and J. L. Haan, **14** (6), 834-841 (2014).
37. B. Ulas, A. Caglar, S. Yılmaz, U. Ecer, Y. Yilmaz, T. Sahan, and H. Kivrak, *International Journal of Energy Research,* **43** (15), 8985-9000 (2019).
38. H. Wang and H. D. Abruña, *Journal of the American Chemical Society,* **139** (20), 6807-6810 (2017).
39. L. Q. Wang, M. Bellini, J. Filippi, M. Folliero, A. Lavacchi, M. Innocenti, A. Marchionni, H. A. Miller, and F. Vizza, *Applied Energy,* **175** 479-487 (2016).
40. X. Yu and A. Manthiram, *Applied Catalysis B: Environmental,* **165** 63-67 (2015).
41. Z. Pan, H. Zhuang, Y. Bi, and L. An, *Journal of Power Sources,* **437** 226944 (2019).
42. S. Luo, Y. Wang, T. C. Kong, W. Pan, X. Zhao, and D. Y. C. Leung, *Journal of Power Sources,* **490** 229526 (2021).
43. L. Han, J. González-Cobos, I. Sánchez-Molina, S. Giancola, S. J. Folkman, S. Giménez, A. Vidal-Ferran, and J. R. Galán-Mascarós, *Sustainable Energy & Fuels,* **4** (12), 6227-6233 (2020).
44. N. Zhang, F. Chen, and L. Guo, *Physical Chemistry Chemical Physics,* **21** (40), 22598-22610 (2019).
45. J. Zheng, H. Zeng, C. Tan, T. Zhang, B. Zhao, W. Guo, H. Wang, Y. Sun, and L. Jiang, *ACS Sustainable Chemistry & Engineering,* **7** (18), 15354-15360 (2019).
46. D. Bhalothia, P.-C. Chen, C. Yan, K.-W. Wang, and T.-Y. Chen, *The Journal of Physical Chemistry C,* **124** (4), 2295-2306 (2020).
47. H. Xiang, H. A. Miller, M. Bellini, H. Christensen, K. Scott, S. Rasul, and E. H. Yu, *Sustainable Energy & Fuels,* **4** (1), 277-284 (2020).
48. X.-Y. Fan, Z. Jiang, L. Huang, X. Wang, J. Han, R. Sun, L. Gou, D.-L. Li, and Y.-L. Ding, *ACS Appl Mater Interfaces,* **12** (18), 20344-20353 (2020).
49. U. Shamraiz, Z. Ahmad, B. Raza, A. Badshah, S. Ullah and M. A. Nadeem, *ACS Appl Mater Interfaces,* **12**, 4396-4404 (2020).
50. L. Preda, N. Spataru, J. M. Calderon Moreno, S. Somacescu and M. Marcu, Electrocatalysis, **11**, 443-453 (2020).
51. Y. Devrim and A. Albostan, Journal of Electronic Materials, **45**, 3900-3907 (2016).
52. V. Galvan, K. Domalaon, C. Tang, S. Sotez, A. Mendez and M. Jalali-Heravi,

Electrophoresis, **37** 504-510 (2016).
53. X. Y. Su, Z. F. Pan and L. An, International Journal of Energy Research, **43** 7433-7443 (2019).
54. L. H. Lan, W. Yang, J. Li, L. Zhang, Q. Fu and Q. Liao, *ACS Appl Mater Interfaces*, **12** (24), 27095-27103 (2020).

Table 1 Performances of the passive air-breathing formate fuel cells

Fuel	Oxidant	Anode	Cathode	T (°C)	P_{max} ($mWcm^{-2}$)	Ref.
HCOOK	Air	PdAuAg/CNT	Pt/C	25	16	This work
HCOOK	Air	Pd	carbon	25	2.53	[52]
HCOONa	Air	Pd	Pd	25	8.9	[25]
HCOONa	Air	Pd/C	Fe-Co	23	9.9	[53]
HCOONa	Air	Pd	Fe-N	25	10.01	[54]

Table 2 Comparison of the performances of the passive air-breathing formate fuel cell with different anode and cathode catalysts

Anode	Cathode	P_{max} (mW cm^{-2})	V_{ocv} (V)	i_{max} (mA cm^{-2})
PdAuAg/CNT on NF	Pt/C on NF	16	0.98	64
Pd/C on NF	Pt/C on NF	7.3	0.97	30
PdAuAg on NF	Pt/C on NF	6	0.9	26
PdAuAg/CNT on CP	Pt/C on NF	4.2	0.85	20

NF: Nickel foam

CP: Carbon paper

P_{max}: The peak power density

V_{ocv}: Open circuit voltage

i_{max}: The maximum current density

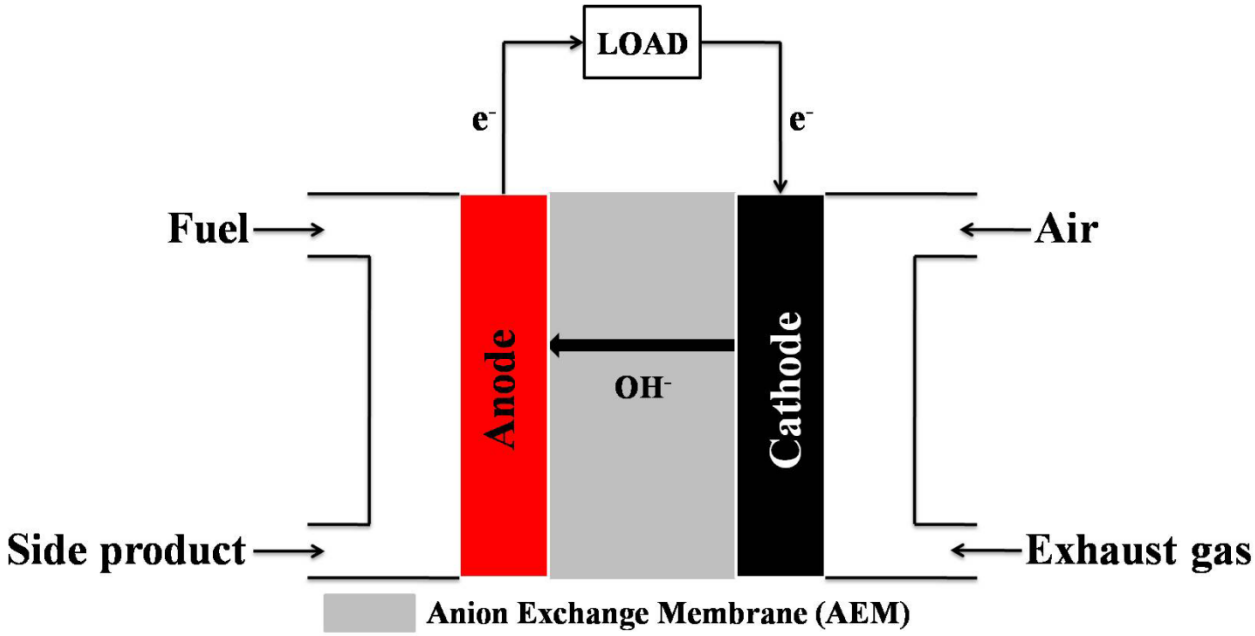

Figure 1. Schematic diagram of the passive air-breathing formate fuel cell.

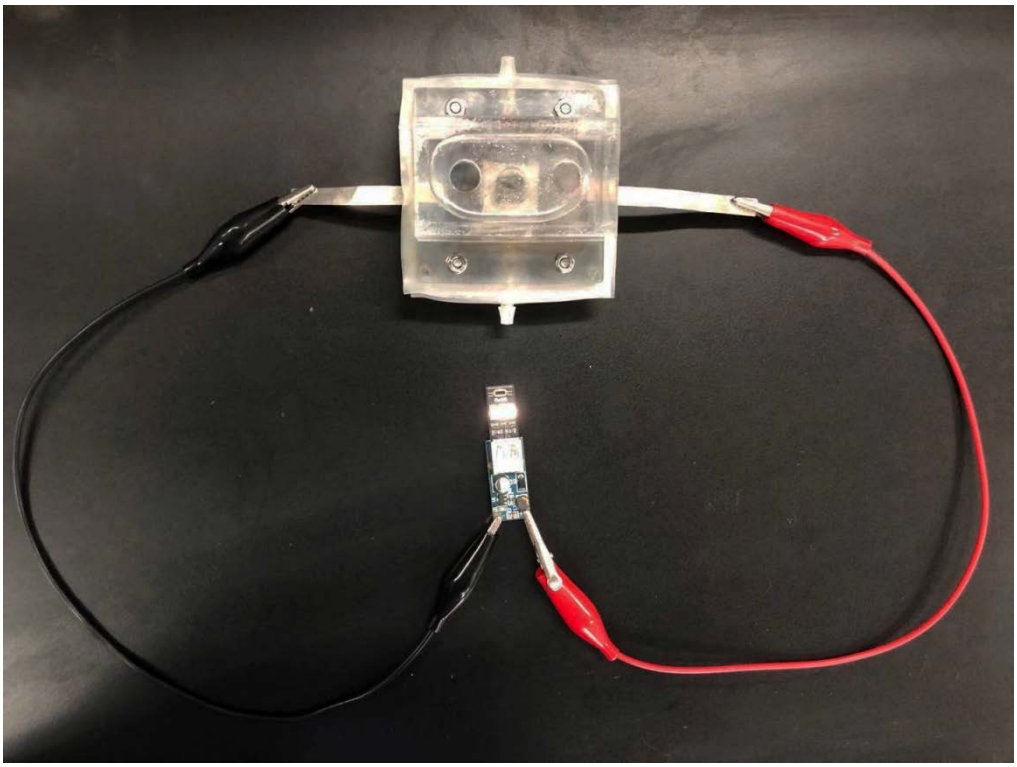

Figure 2. Photograph of the passive air-breathing formate fuel cell.

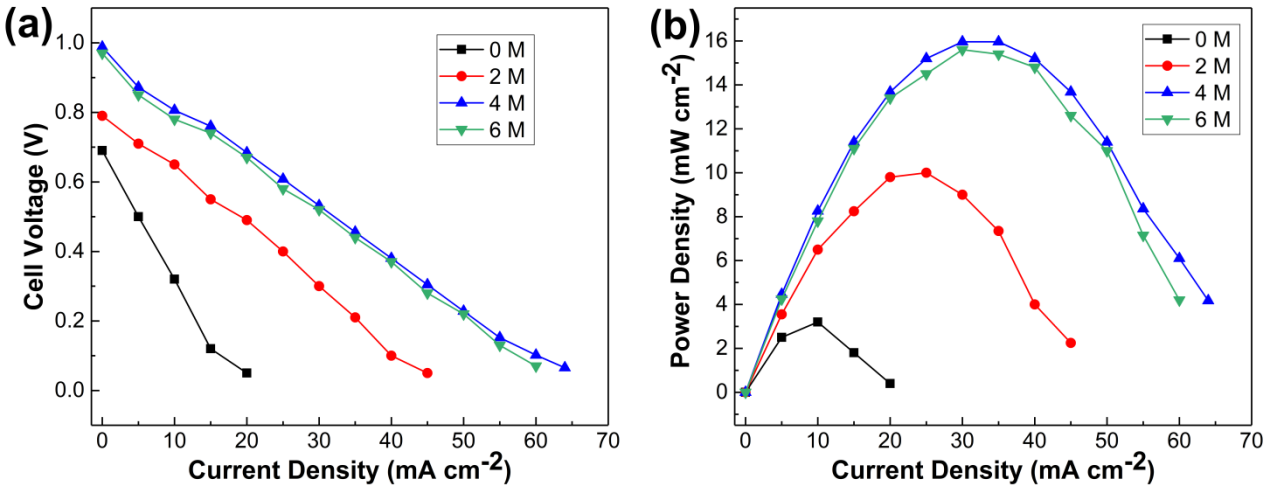

Figure 3. The (a) polarization and (b) power density curves of the passive air-breathing formate fuel cell with different concentration KOH. (Anode loading was 10 mg cm^{-2} PdAuAg/CNT on nickel foam, cathode loading was 10 mg cm^{-2} Pt/C on nickel foam. Anode was KOH + 5 M HCOOK, cathode was air, temperature of fuel and fuel cell was 25 ℃)

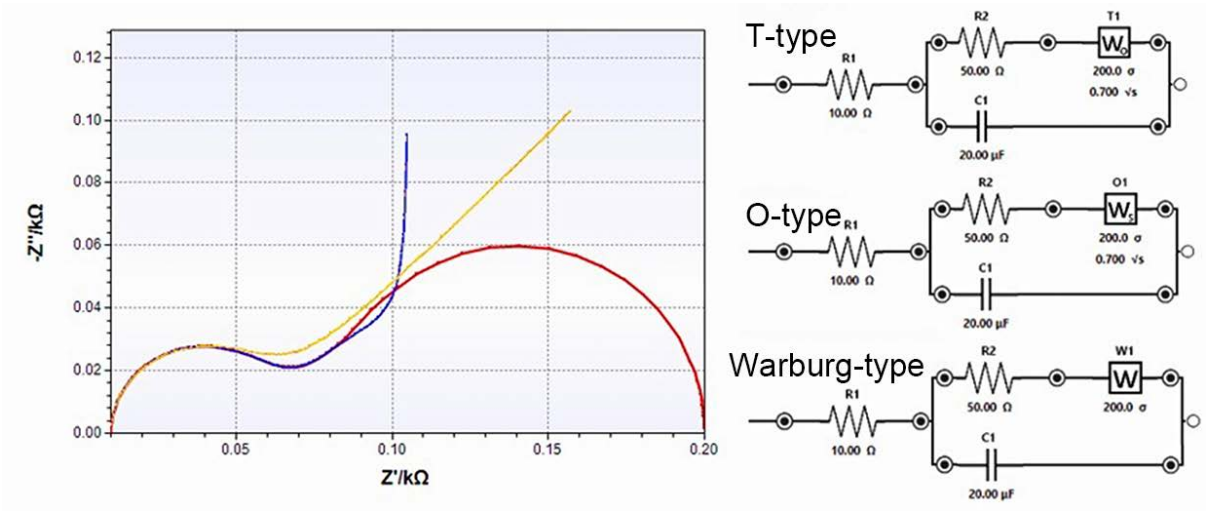

Figure 4. Different curve types of Nyquist plots at low frequency

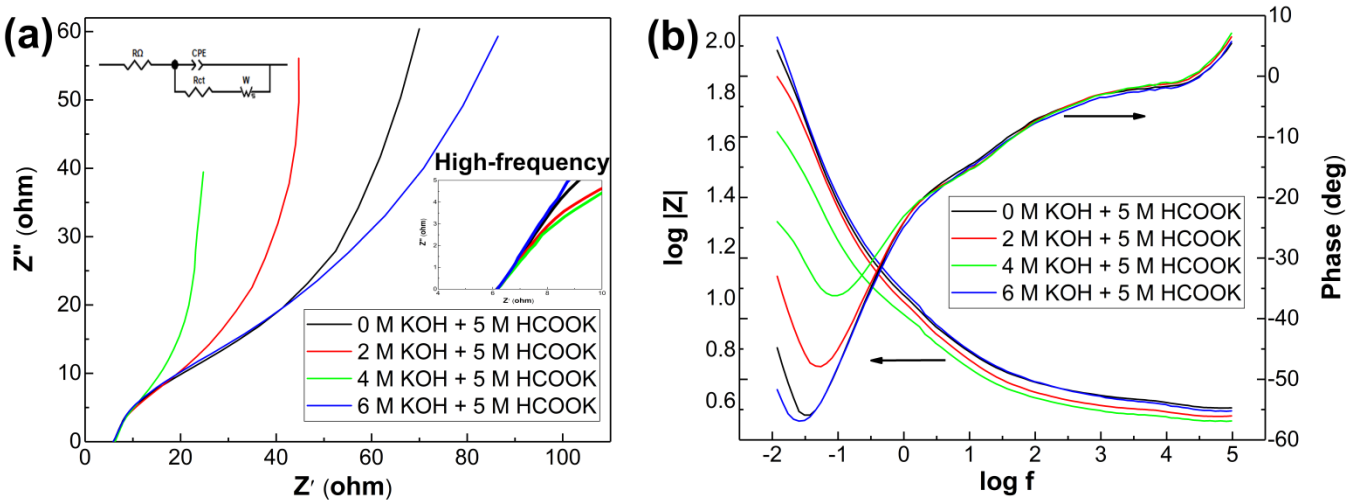

Figure 5. The (a) Nyquist and (b) Bode plots of the passive air-breathing formate fuel cell at various KOH concentrations with 5 M HCOOK as the anode fuel. The inset shows the equivalent electric circuit of fitting the Nyquist plot.

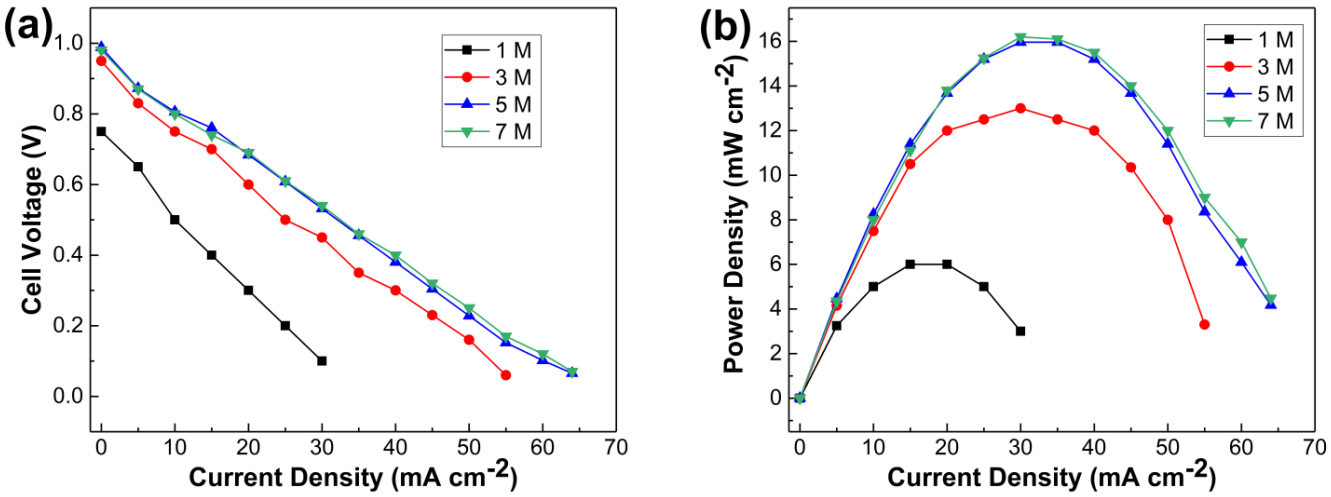

Figure 6. The (a) polarization and (b) power density curves of the passive air-breathing formate fuel cell with different concentration formate. (Anode loading was 10 mg cm^{-2} PdAuAg/CNT on nickel foam, cathode loading was 10 mg cm^{-2} Pt/C on nickel foam. Anode was 4 M KOH + HCOOK, cathode was air, temperature of fuel and fuel cell was 25 ℃)

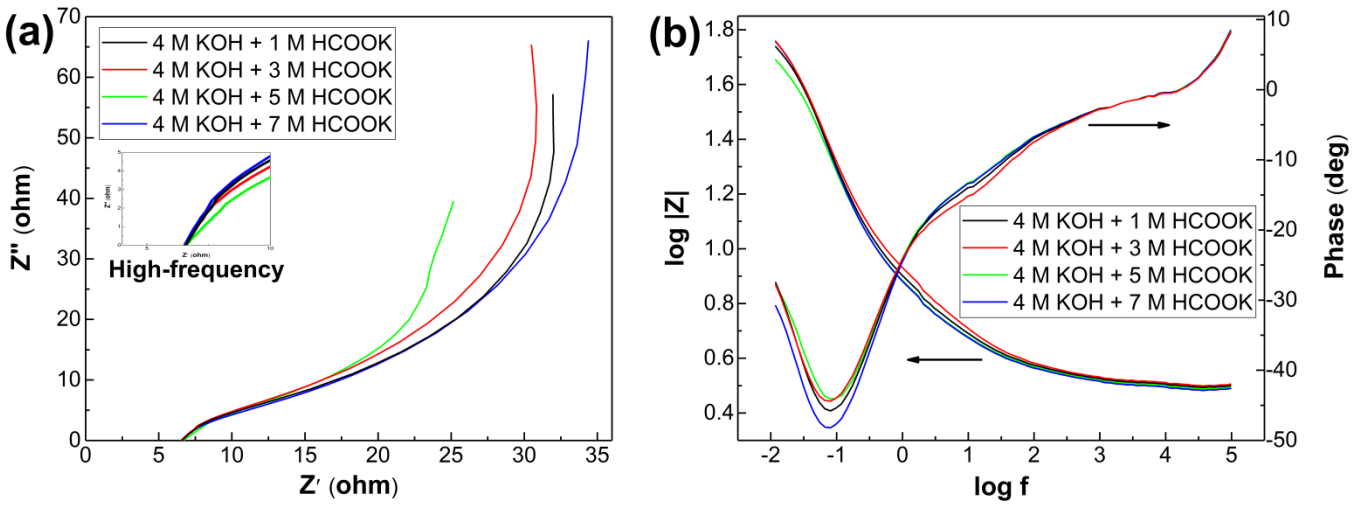

Figure 7. The (a) Nyquist and (b) Bode plots of the passive air-breathing formate fuel cell at various formate concentrations with 4 M KOH as the anode fuel.

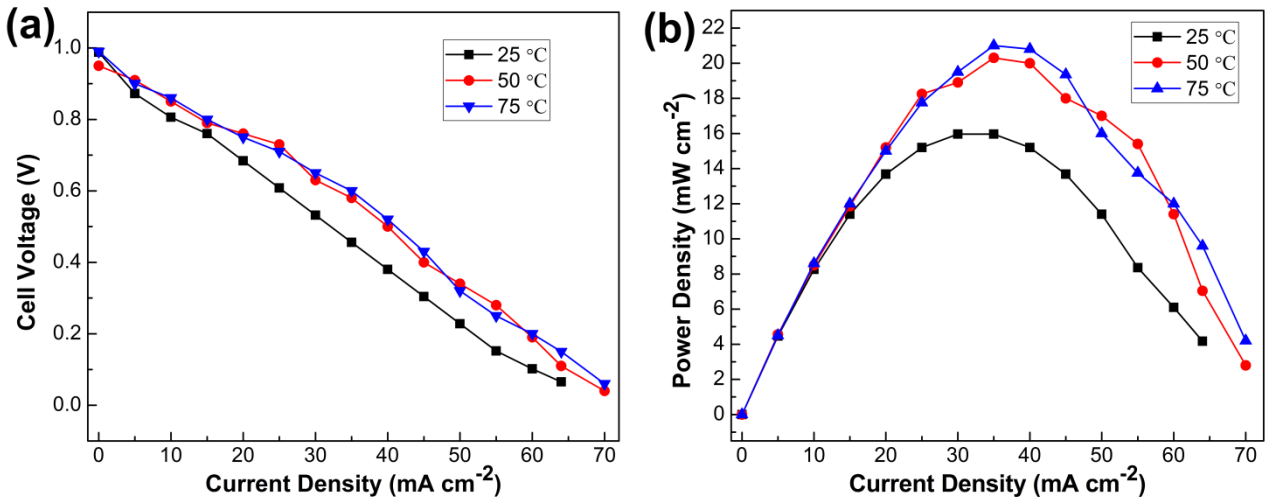

Figure 8. The (a) polarization and (b) power density curves of the passive air-breathing formate fuel cell with different operation temperatures of fuel and fuel cells. (Anode loading was 10 mg cm^{-2} PdAuAg/CNT on nickel foam, cathode loading was 10 mg cm^{-2} Pt/C on nickel foam. Anode was 4 KOH + 5 M HCOOK, Cathode was air)

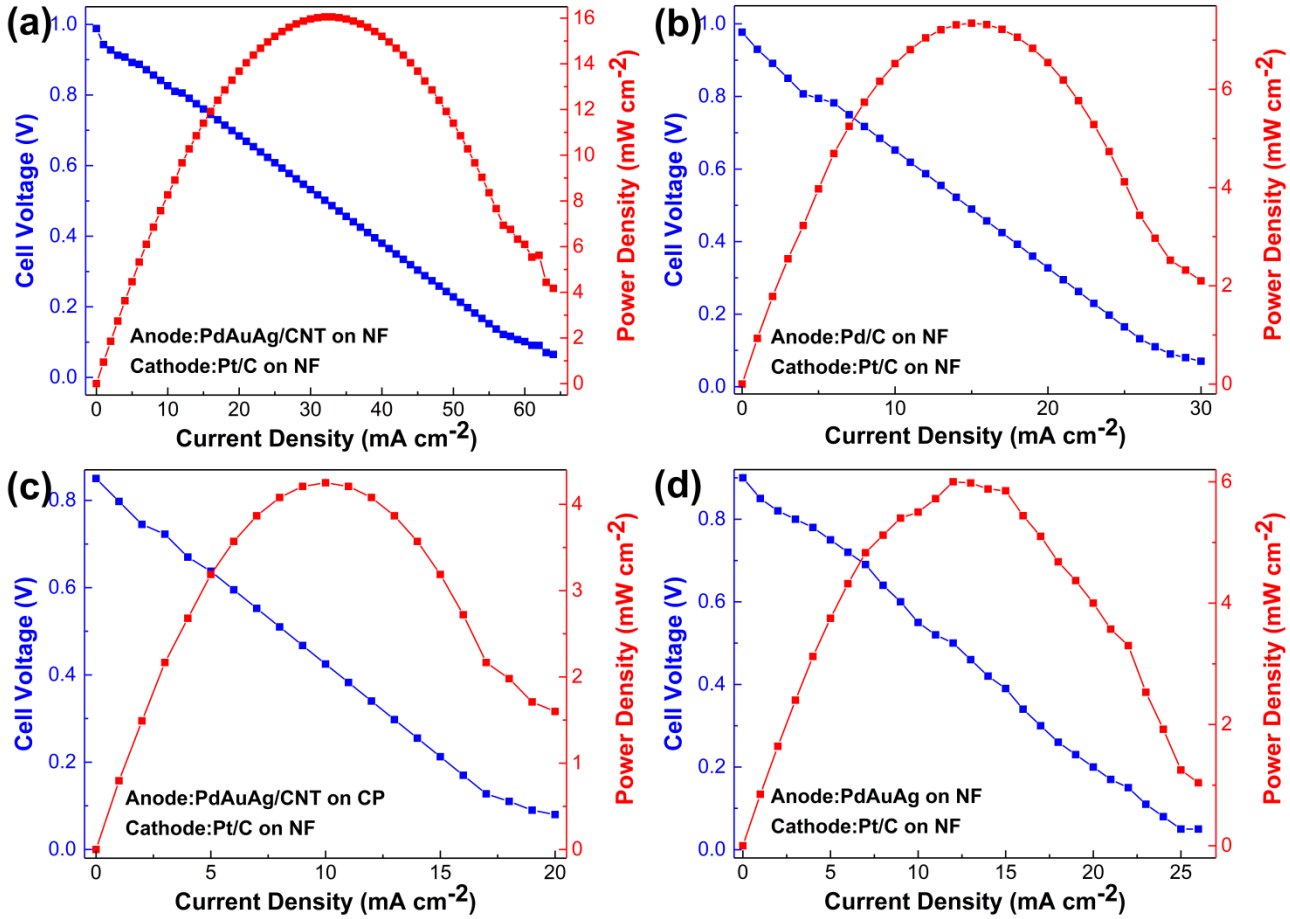

Figure 9. The polarization (V–I) and power density curves of the passive air-breathing formate fuel cell. (a) PdAuAg/CNT on nickel foam as anode and Pt/C on nickel foam as cathode; (b) Pd/C on nickel foam as anode and Pt/C on nickel foam as cathode; (c) PdAuAg/CNT on carbon paper as anode and Pt/C on nickel foam as cathode; (d) PdAuAg on nickel foam as anode and Pt/C on nickel foam as cathode. (Anode loading was 10 mg cm^{-2} PdAuAg/CNT or Pd/C, cathode loading was 10 mg cm^{-2} Pt/C. Anode was 4 M KOH + 5 M HCOOK, cathode was air, temperature of fuel and fuel cell was 25 ℃)

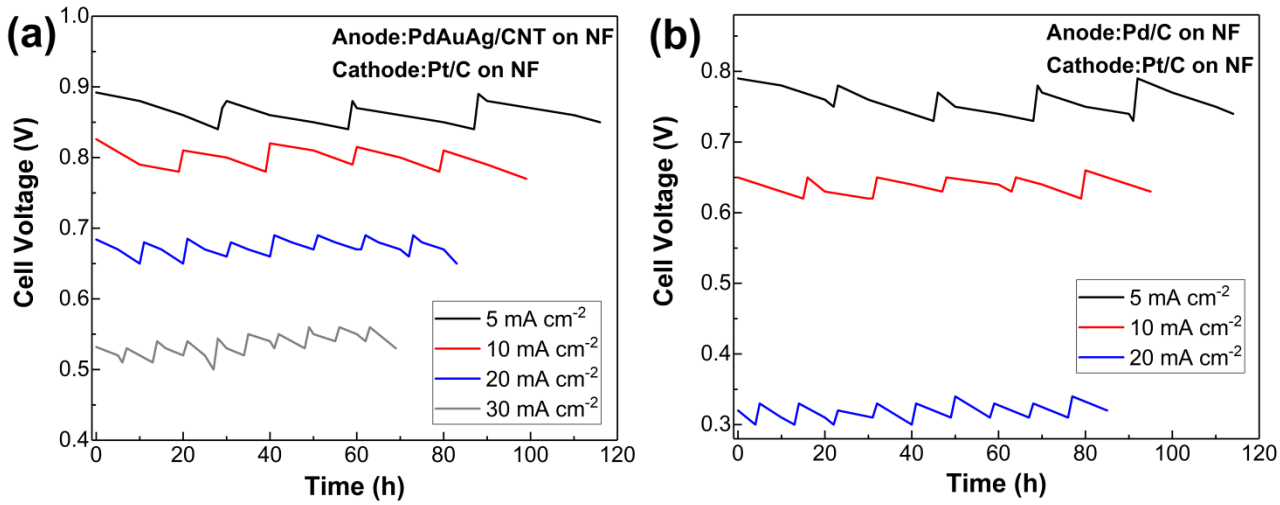

Figure 10. Stability tests at different current densities. (a) PdAuAg/CNT on nickel foam as anode and Pt/C on nickel foam as cathode ; (b) Pd/C on nickel foam as anode and Pt/C on nickel foam as the cathode.